Heavy metal oxide glass-ceramics containing luminescent gallium-garnets single crystals for photonic applications

A. E. Souza, S. G. Antonio, Sidney J. L. Ribeiro, Douglas Faza Franco, Gustavo Galeani, Thierry Cardinal, Marc Dussauze, Marcelo Nalin

Heavy metal oxide glass-ceramics containing luminescent gallium-garnets single crystals for photonic applications

A. E. Souza[a], S. G.Antonio[a], Sidney J. L. Ribeiro[a], D. F.Franco[a], G. Galeani[b], T. Cardinal[c], M. Dussauze[d], M. Nalin[a]

[a] *Institute of Chemistry – São Paulo State University – UNESP, Araraquara, SP, Brazil*
[b] *São Carlos Institute of Physics, University of São Paulo, São Carlos, SP, Brazil*
[c] *University of Bordeaux, CNRS, ICMCB, UPR 9048, Pessac, France*
[d] *University of Bordeaux, CNRS, ISM, UPR 5803, Pessac, France*

Abstract: Glass-ceramics containing rare earth gallium garnets were obtained using glass compositions as reactional medium. This work reports on the synthesis, and structural, morphological, and optical characterizations of Er^{3+} and Tm^{3+}-doped $Yb_3Ga_5O_{12}$ crystals prepared from controlled cooling of heavy metal oxide glass melts. Micrometric cubic crystals were obtained by controlling the cooling of a rare earth-supersaturated glassy composition melted at high temperature. Crystals with sizes ranging between 5 and 150 µm were formed into the glass matrix. A gallium garnet phase corresponding to space group *Ia*-3*d* was identified by X-ray diffraction and confirmed by Rietveld simulations. The morphology of crystals was studied by optical and scanning electron microscopies, while chemical elements were mapped by electron dispersive X-Ray spectroscopy. The glass phase was studied by XRD, thermal analysis and Raman spectroscopy. The optical properties of both glass and glass-ceramic materials were evaluated by UV–Vis and luminescence spectroscopies. Micro-luminescence measurements confirmed that rare earths were incorporated into the crystalline phase. Intense upconversion emissions of Er^{3+} (550 and 660 nm) and Tm^{3+} (800 nm) were observed when the glass-ceramics were pumped at 980 nm. These new glass-ceramics are excellent candidates for the development of photonic devices.

Keywords: Glass-ceramics ; Glass matrix composites ; Gallium garnet ; Luminescence ; Rare earths

1. Introduction

Glasses containing rare earth ions have been studied as emitters in optical amplifiers [1], optical thermometers based on upconversion effects [2], white light generation [3], [4] among other applications. In particular, glass-ceramics prepared from glasses by controlled thermal treatment allows to explore properties like those of single crystals. The growth of optically active crystals into a glassy matrix however is a challenge, because the homogeneity and transparency of glass-ceramics have to be sustained while luminescent ions are incorporated in the crystal phase. Several glasses have been used for such purposes, but each one has its own peculiarities. Moreover, cubic phases are preferred for avoiding anisotropy induced by preferential orientations of crystals into the glassy matrix. In this work, heavy metal oxide glasses were studied due to their set of interesting properties, such as low phonon energy, good infrared transparency, high refractive index (higher than 2), good chemical stability, among others, making them excellent as photonics.

Recently, several papers have disclosed the interesting properties of $RE_3Ga_5O_{12}$ garnets (RE = rare earths) [5], [6]. Almost all rare earths can be used to explore both optical [7] and magnetic properties of these garnets

[8]. Most of reports described the synthesis of these materials as polycrystalline nanosized powders or sub micrometer single crystals by solid state reactions, solution combustion and sol-gel methods [7], [9], [10], [11].

The synthesis of new glass compositions and the comprehension about the thermodynamic of crystal growth, mainly concerning the kinetic behavior, have allowed for the preparation of special glass-ceramics. Luminescent crystals embedded in heavy metal oxide glass are of great interest for the development of efficient amplifiers or powerful solid-state lasers [12], [13]. A triple-doped glass (Yb^{3+}, Er^{3+} and Tm^{3+}) was studied herein because the combination of these rare earths has been found to result in white light generation due to a well-known energy transfer upconversion mechanism [14], [15]. In this work, we studied how changes in the chemical composition of heavy metal oxide glasses influence the formation of highly luminescent glass-ceramics. Both glasses and glass-ceramics were characterized by thermal analysis, Differential Scanning Calorimetry (DSC), X-ray diffraction, micro-Raman, micro-luminescence and UV-Vis spectroscopies, optical microscopy (OM), scanning electron microscopy (SEM), and energy-dispersive X-ray spectroscopy (EDS).

2. Experimental details

The following analytical grade raw materials were used: GeO_2 (99.999%), Ga_2O_3 (99.99%) and Bi_2O_3 (99.975%) from Alfa Aesar, PbO (99.0% - Fluka), Tm_2O_3 (99.9957%), Er_2O_3 (99.9695%), and Yb_2O_3 (99.9987%) from REEtec.

Multicomponent heavy metal oxide glasses with molar composition 40PbO-20GeO_2-25Bi_2O_3-15Ga_2O_3 and 97(40PbO-20GeO_2-25Bi_2O_3-15Ga_2O_3)-2Yb_2O_3-0.5-Er_2O_3-0.5-Tm_2O_3 (in mol%), here called PGBG and PGBG6, respectively, were studied. The glass samples were obtained by a melt-quenching process, in which the raw materials were weighed, homogenized in a speed mixer equipment, transferred to a Pt/Rh crucible, and melted in a conventional furnace. The melts without rare earths were kept at 1200 °C for 40 min for full homogenization, and then poured into a pre-heated steel-brass mold at 350 °C, where they were annealed for 3 h to eliminate internal stresses due to thermal shock. Afterwards, the furnace was turned off and the samples were allowed to cool down to room temperature.

The glass-ceramics were prepared by the addition of rare earths to the glass compositions. To prepare the glass-ceramics, the melts were cooled into the pre-heated steel-brass mold at 350 °C. To obtain the crystal-free glasses containing rare earths, the melts were cooled between two plaques kept at room temperature (fast quenching rate). On the other hand, when the melts were cooled out of the furnace to room temperature, into the crucible, fully crystallized samples were obtained (slow quenching rate).

The bulk glass and glass-ceramic samples were polished using ethyl alcohol and silicon carbide (SiC - Struers) sieves, with decreasing grain size of 800 (20–24 µm), 1200 (13–16 µm), 2400 (7–10 µm), 4000 (<6 µm), and finally with 0.5 and 0.3 µm alumina suspensions for improving their optical quality.

The samples were characterized by X-ray diffraction (XRD) using a Bruker D8 Advance diffractometer with Cu kα radiation (1.54 Å) in the range of 2(θ) from 2° to 70°, Soller slit 2.5°, divergence slit 0.2° and pass of 0.02°. Thermal analysis (DSC) were done in a NETZSCH 404F3 Pegasus equipment in the range from 300 to 600 °C under N_2 atmosphere at a flow rate of 20 mL min^{-1} and heating rate of 10 °C min^{-1} using platinum crucibles. The analyses were performed using around 15 mg of sample. The characteristic temperatures: glass transition temperature (T_g) and onset of crystallization (T_x) were determined. The stability parameter (T_x-T_g) was used to compare the stability against devitrification between samples. The errors associated with the determinations of Tg and Tx were±2 °C.

Micro-Raman spectra were obtained using a Horiba Jobin Yvon LAB Ram HR spectrometer using a laser with λ = 632.8 nm, slit of 100 µm, and objective of x50WD in the range from 200 to 1500 cm^{-1}.

Micro-luminescence measurements were recorded in backscattering mode on a micro-Raman spectrometer HR800 (Horiba/Jobin Yvon). As excitation source, a continuous wave laser operating at 638 nm and a pulsed picosecond laser of 1064 nm were used. Typical spectral resolution used for Raman is 2.5 cm^{-1}. The objective used was a 100x long working distance with a numerical aperture of 0.5 from Mitutoyo allowing a resolution in the X-Y plane of 0.8 µm.

Emission spectra were obtained in the range from 250 to 850 nm using a Horiba Jobin Yvon spectrophotometer equipped with a R928 Hamamatsu photomultiplier and excited by a diode laser operating at 980 nm. The UV–Vis spectra were obtained using a Cary 5000 – Varian spectrometer in the range from 350 to 2000 nm in the transmission mode.

Scanning electron microscopy (FEG-SEM) analyses were done using a JEOL microscope model 7500F. Chemical analysis were obtained using EDS and elemental mapping on bulk samples covered with gold, using a detector ThermoFisher Scientific Ultra Dry with voltage of 10.0 kV and take off angle of 49.1°.

Optical images were collected using an optical microscope model Leica DM2500M with lens 5, 10, 20 e 50x. To obtain the images, the glass samples were polished to expose the crystal faces.

3. Results and discussion

Melt-quenching is the most common technique used to obtain completely amorphous glasses. In this work, this technique was combined with the chemistry of supersaturated solutions. First, the heavy metal oxide glass composition was chosen to obtain samples with high transparency from the visible up to medium infrared region. As a second step, we studied the upper limit rare earth content that could be incorporated in the glass matrix without inducing its complete crystallization. In practical terms, the synthesized glass containing rare earths should be transparent to the eyes, without visible light scattering. In the last step, we studied the synthesis conditions, in specific the difference between the melting and mold temperatures, thus controlling the quenching rate, as well as the annealing times.

Based on the steps described above, the chemical composition 40PbO-20GeO_2-25Bi_2O_3-15Ga_2O_3 was chosen as the passive host while the composition 97(40PbO-20GeO_2- 25Bi_2O_3-15Ga_2O_3)-2Yb_2O_3-0.5-Er_2O_3-0.5Tm_2O_3 was the active one. The concentration of rare earths (3 mol% in total) was above the limit to obtain the completely amorphous glassy phase, in other words, this concentration represents a supersaturated condition. Both glass and glass-ceramic samples were characterized, as discussed below.

Fig. 1a shows photographs of the PGBG and PGBG6 samples. Visually, no macro-differences were observed, and both samples seemed to be transparent. However, optical microscope observations revealed the presence of cubic crystals ranging from 5 to 100 µm in the glass-ceramic sample, Fig. 1b (bottom), while the sample PGBG (top) did not show any trace of crystalline phases within the same scale. In Fig. 1c, it is shown a detailed image of the cubic crystals. This image will be used latter in the text to discuss the luminescence properties of both crystals and glasses.

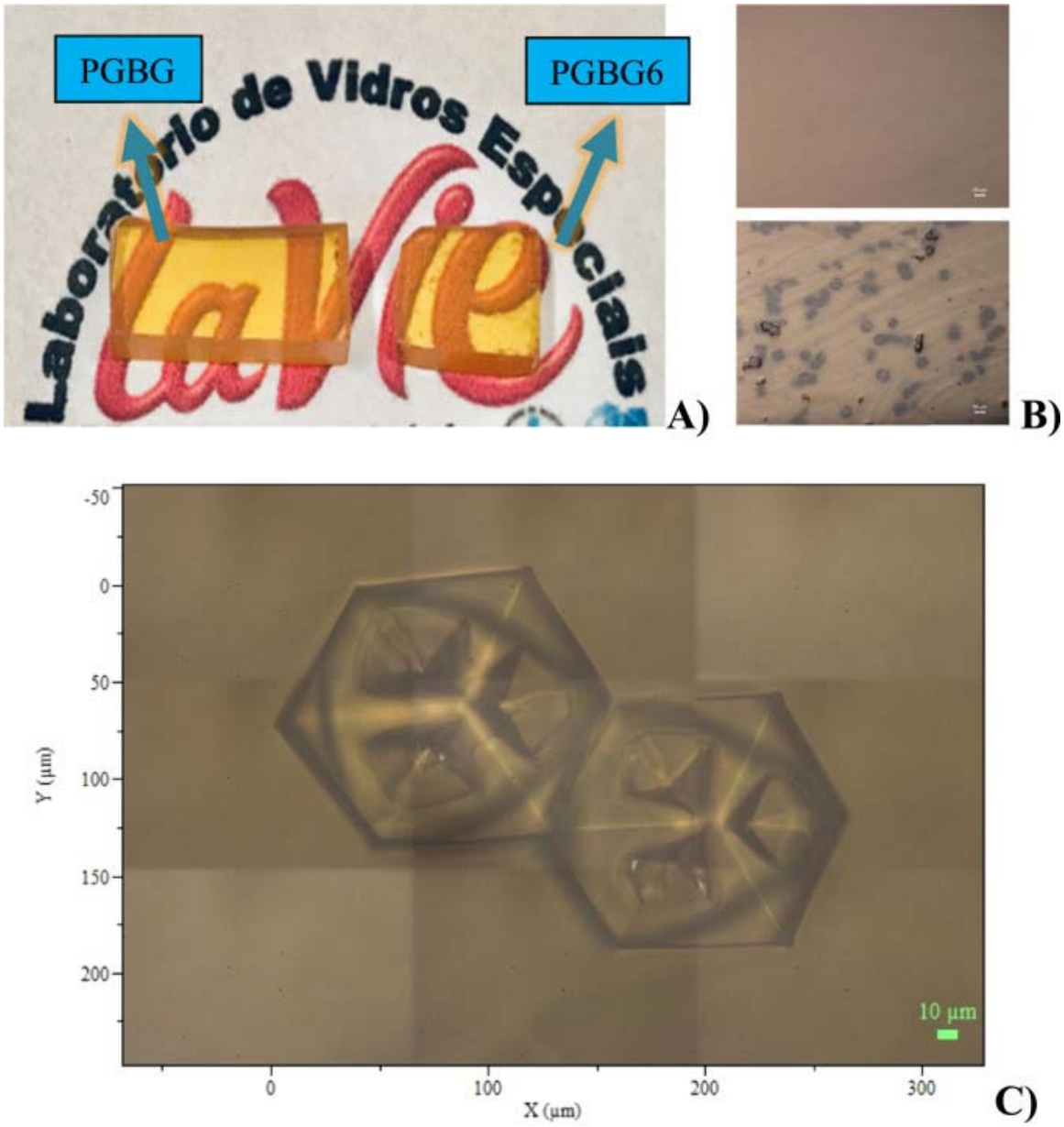

Fig. 1. A) Photographs of glass (PGBG) and glass-ceramic (PGBG6) samples. B) Optical microscopy images of glass PGBG (top) and glass-ceramics PGBG6 (bottom) with lens x10 (scale bars correspond to 50 µm). C) Magnified OM image showing the cubic crystals in detail.

Fig. 2 shows the DSC curves of the glass and glass-ceramic samples. It is possible to ensure that the glass phase was present in both samples. A Tg was observed at 379 °C for PGBG and no Tx and Tp (temperature of maximum crystallization) were observed in the temperature range analyzed. The PGBG6 sample displayed Tg at 390 °C due to addition of rare earth ions. No evidence of further crystallization was observed up to 600 °C, thus it is possible to affirm that the thermal stability parameter (Tx-Tg) was higher than 200 °C for both samples.

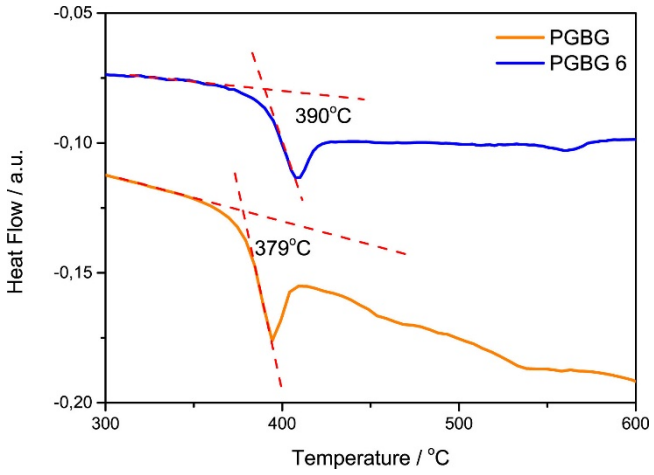

Fig. 2. DSC curves of PGBG and PGBG6. Tg values were obtained as the interception between two tangent dashed lines.

Due to the fact that the glassy phase is not detected by XRD, resulting only in a halo characteristic of amorphous materials (insert in Fig. 3), the discussion about the X-ray diffraction data was done using the glass-ceramic sample. Fig. 3 shows the X-ray diffraction profile of the glass-ceramic sample along with the simulated pattern. It can be observed a halo centered at 29° due to the amorphous phase, and narrow diffraction peaks at 18°, 36° and 56° of 2θ. From the XRD measurements, it was possible to identify the crystal phase using the Rietveld method (TOPAS-Academic v6.0). Data refining confirmed that the obtained phase is due to the crystalline phase of $Yb_3Ga_5O_{12}$ (PDF-ICDD: 73-1373) with space group *Ia*-3*d*. The amorphous fraction was corrected with the background using the Chebyshev function. The unit cell was refined, and the cell parameter obtained was a = 12.229(2). The preferred orientation was corrected with the March Dollase model.

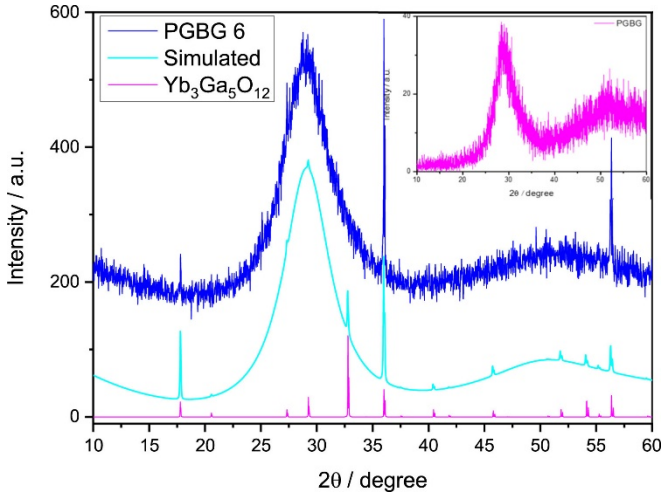

Fig. 3. Experimental (blue-PGBG6), simulated (light blue) and reference (PDF-ICDD: 73-1373) (pink-$Yb_3Ga_5O_{12}$) diffractograms of PGBG6. Insert: XRD pattern of amorphous PGBG.

The results were also compared with those of germanium garnet phases. Several crystalline phases based on the generic structure $A_3B_2Ge_3O_{12}$ (with A= twofold cations and B= threefold cations) have been reported in the literature [16]. Since these compounds can also form cubic structures with the same space group, *Ia*-3*d*, it was necessary do discuss them to justify the formation of gallium instead germanium garnets in the samples prepared herein. First, it is worth pointing out that the chemical composition of the PBBG6 glass would allow the $Pb_2Ga_3Ge_3O_{12}$ compound to be formed. However, the crystallographic parameters of this phase were not found in the literature. A similar compound with chemical composition $Ca_2Ga_3Ge_3O_{12}$ presents the same specifications of gallium garnets, including a lattice parameter

a = 12.251 Å. This value is close to that obtained in this work (the effective ionic radii of Ca^{2+} and Pb^{2+} are 100 pm and 119 pm, respectively, thus it is necessary to consider some changes in the *a*-value). Table 1 summarizes the data of all discussed compounds. It can be observed that all crystals exhibited the same space group and the a-values fluctuated from 12.204 Å for $Yb_3Ga_5O_{12}$ to 12.255 Å for $Er_3Ga_5O_{12}$, depending on the ionic radius of each rare earth.

Table 1
Rietveld simulation results for PGBG6 and published reference materials.

	PDF number	System	Space Group	A (Å)
PGBG6		*cubic*	*Ia-3d*	*12.229(2)*
$Er_3Ga_5O_{12}$	12-769	cubic	Ia-3d	12.255
$Tm_3Ga_5O_{12}$	23-589	cubic	Ia-3d	12.228
$Yb_3Ga_5O_{12}$	73-1373	cubic	Ia-3d	12.204
$Ca_3Ga_2Ge_3O_{12}$	ICSD1123	cubic	Ia-3d	12.225[a]

[a] Please, see Ref. [16].

Due to similarities in packing structure and lattice parameters, it was quite difficulty to confirm the rare earths distribution within the crystals. However, there was strong evidence that all rare earth ions were included both in the glassy and crystalline phases, as shown below.

Fig. 4 represents the 3D unit cell and its packing for the formation of crystalline structures. The $RE_3Ga_5O_{12}$ structure may be generically described by GaO_6 and GaO_4 polyhedra linked by an oxygen atom, forming 3D chains along the network, and creating dodecahedral cavities occupied by rare earth atoms [7].

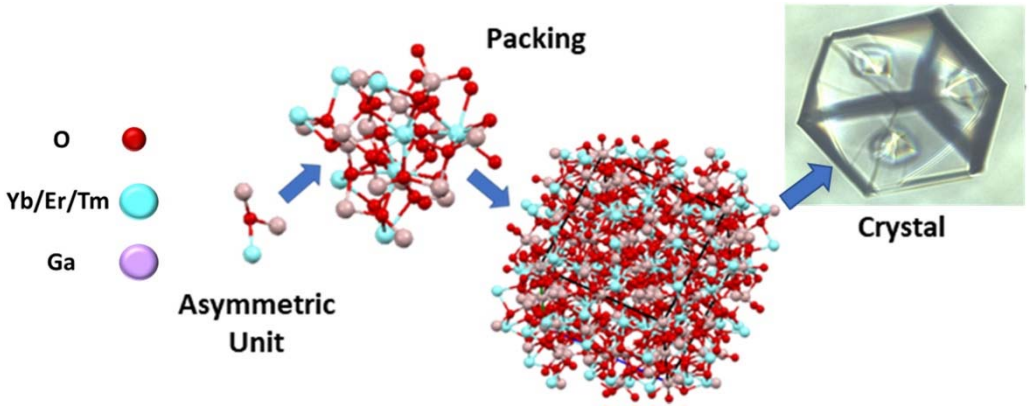

Fig. 4. 3D representation of crystal growth obtained by molecular modeling from PDF-ICDD: 73-1373 data using the Mercury software.

The distribution of chemical elements in the PGBG6 sample was studied by EDS and SEM elemental mapping, and the results can be seen in Figs. 5 and 6, respectively. These measurements were done after polishing the glass-ceramic until one crystal surface was exposed. The EDS results strongly indicated that the chemical composition of crystals mainly contained Ga rather than germanium. The energies of both atoms were similar, however, as shown in detail in Fig. 5, it was possible to identify the presence of Ga at 0.95 (edge L_1) and 1.098 keV (edge L_{a1}) as the most intense peaks, while the Ge signal at 1.19 keV (edge La_1) was only observed as a shoulder. Also, a signal ascribed to Yb^{3+} is noted at 1.19 keV (edge Mz_I). This fact supports the formation of gallium garnet structures. The electronic transitions arising from the three rare earths could be identified between 1.3 and 1.6 keV. The signals at 2.33 and 2.42 keV were ascribed

to possible transitions of Pb and Bi, respectively. However, such transitions may overlap with those of gold, which was used to coat the sample. It was assumed that both, Pb and Bi, were absent in the samples, once the elemental mapping, shown in Fig. 6, rules out the presence of such ions into the crystals. These results confirm the formation of the gallium garnet phase in the glass-ceramics.

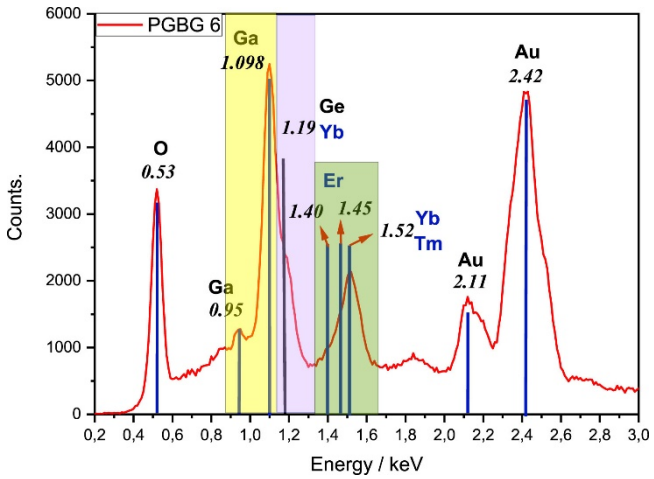

Fig. 5. SEM-EDS spectrum of crystal surface.

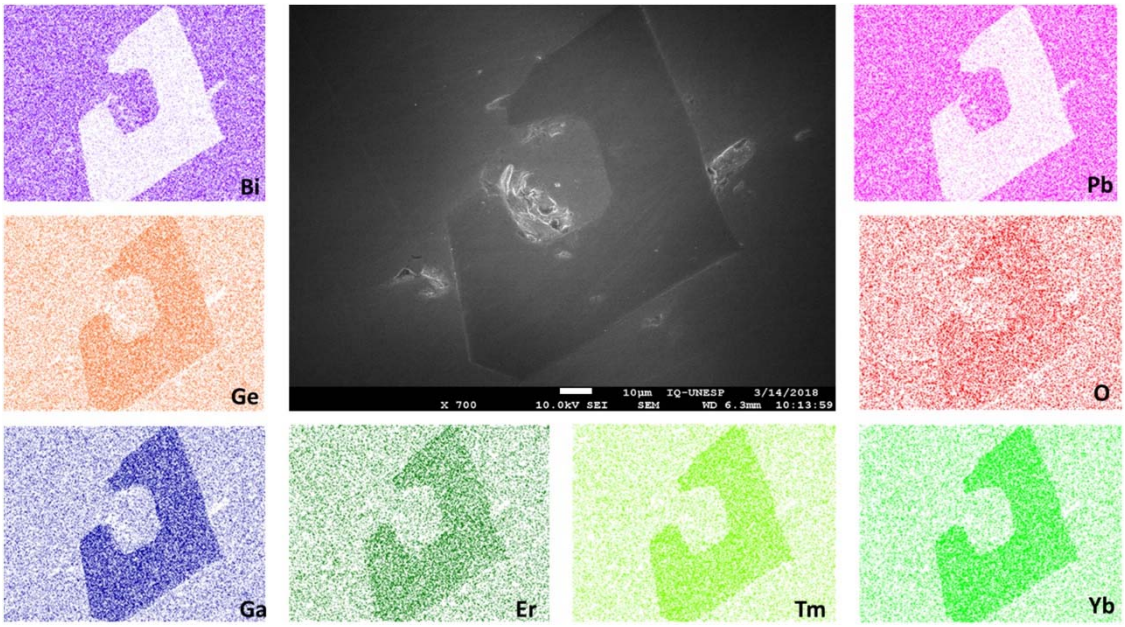

Fig. 6. SEM image and elemental mapping results of PGBG6. The darker part in the SEM image corresponds to the crystal, while the lighter part relates to the glassy phase. The map of each element is displayed along with its chemical symbol.

The darker region in the center of the SEM image corresponds to the crystal, while the lighter region is ascribed to the glass. Fig. 6 reveals the distribution of chemical elements contained in both phases. The dark region is predominantly composed of Ge, Ga, and the three rare earths (Yb, Er and Tm). The presence of Ge and Ga in the crystal is due to the fact that these elements have close atomic numbers and, consequently, their transitions are similar, making difficult to separate both signals. Thus, combining these data with those from Rietveld refinement and EDS, it is possible to confirm that gallium is present in the crystals. The same analogy is done for the rare earth ions, since these elements are neighbors in the periodic table, thereby exhibiting similar transitions. Accordingly, the elemental maps indicated the presence of Yb, Er and Tm. As will be discussed below, the luminescence data indicated that the three REE

were incorporated in the crystals. However, we also observed that these elements were dispersed in the entire sample surface because the crystallization occurred only partially, and as a result, a fraction of REE remained in the glassy phase.

In the OM image shown in Fig. 4, the cubic crystals seem to be partially filled, since holes at their surface are noticeable. These features were also observed by SEM. Such a behavior will be explained in detail below using the micro-luminescence measurements.

Raman spectroscopy was used to collect further structural information and study the influence of rare earths on the glass arrangement. Fig. 7 shows the Raman spectrum of PGBG. As expected for a glassy material, large bands are observed enveloping all contributions of Ge-O, Ga-O, Bi-O and Pb-O bonds. The Raman spectrum is similar to other germano-gallate glasses [14], [15], [17], [18], [19], [20], [21] with predominant absorption bands around 400 and 750 cm^{-1}. The deconvolution analysis was done based on methods reported elsewhere [19], [22], [23], [24] and all band assignments are summarized in Table 2.

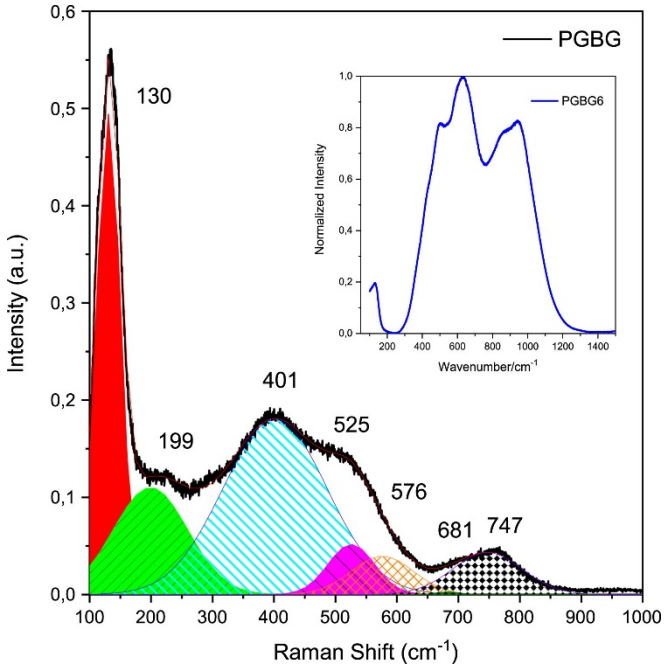

Fig. 7. Raman spectrum and Gaussian deconvolution of PGBG. Inset: Raman spectrum of PGBG6 corresponding to emissions of rare earth ions under excitation at λ = 632.8 nm.

Table 2
Raman band assignments after deconvolution of PGBG glass sample.

Sample	Wavenumber (cm^{-1})	Assignment	References
PGBG	130	BiO6 or PbOn (n = 3,4)	[22,23]
	199	Bi-O or Pb-O (group modes)	[22,23]
	401	Ga(Ge)-O-Pb or Ga(Ge)-O-Bi	[22]
	525	Ga(Ge)-O-Ga(Ge)	[22,24]
	576	Ga(Ge)-O-Ga(Ge)	[22,24]
	681	Ga(Ge)-O-	[19,22–24]
	747	Ga(Ge)-O^-	[19,22–24]

The bands at 130 cm^{-1} and 199 cm^{-1} (group modes) relate to BiO_6 or PbO_n units. The signals of each unit were difficult to separate due to the similarities between the GeO_4 and GaO_4 polyhedra, thus both contributions were treated together and called as Ga(Ge)[23]. The band around 400 cm^{-1} corresponds to bonds from Ga(Ge)-O-Bi (or Pb), whereas the bands between 525 and 576 cm^{-1} are associated with vibrations of GaO_4 and GeO_4 polyhedra. At higher frequencies, we identified the stretching modes of Ga(Ge)-O^- involving non-bridging oxygen [19], [24].

The inset in Fig. 7 shows the Raman spectrum of the sample containing rare earths. It is evident that the vibrational spectrum could not be explained because the Raman photodetector is much more sensitive to emissions from the rare earths than those arising from the vibrations. Other measurements using a laser with λ = 1064 nm were done to overcome such an inconvenience, but emissions from Tm^{3+} ions became significant at this wavelength and no spectra from the vibrational part were observed.

On the other hand, micro-luminescence signals arising from the crystal and glass phases were collected and mapped using the Raman spectrometer, as displayed in Fig. 8. The emission from both phases were in accordance with the elemental mapping results. For the spectrum collected on the glass phase surface, which contained no crystals, the emission curves were typical of amorphous materials. However, when the spectrum was taken from the crystal phase surface, the emission was similar to those arising from crystals, in which the stark levels from Er^{3+} ions are more evident [25], [26]. The main emissions were depicted as the energy level diagram in the insert of Fig. 8a. Using the Raman mapping mode, it was possible to generate 3D images of the cubic crystals. As seen in Fig. 8b, the crystal luminescence was z-dependent. More importantly, and corroborating with the SEM mapping (Fig. 6), the cubic crystals were confirmed not to be fully organized and the amorphous phase (glass) was present at their center. The emission distribution (from ~650 up to 680 nm) on the cubes shown in Fig. 8 correspond to Er^{3+} ions.

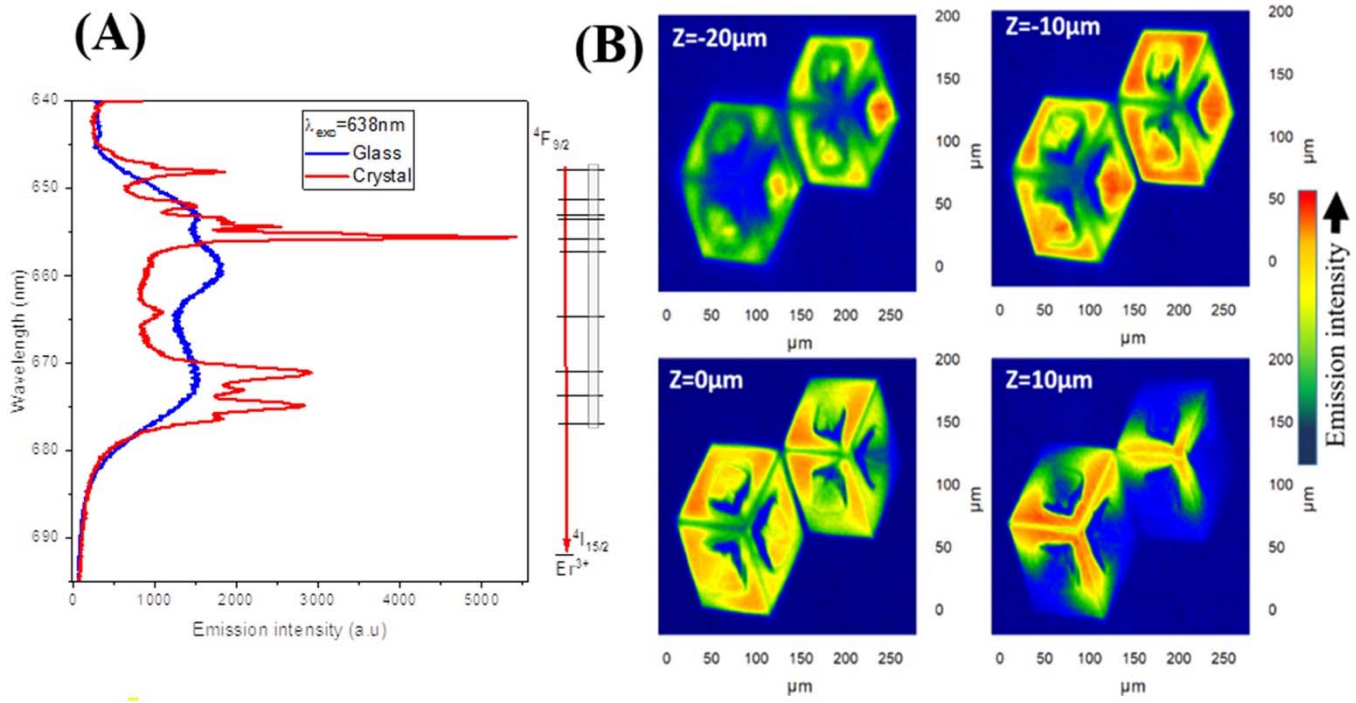

Fig. 8. a) Micro-luminescence emission spectra (downshifting, λ_{exc}= 638 nm) of glass and crystal phases obtained using a Micro-Raman spectrometer and correspondent energy level diagram of Er^{3+} ions. b) Luminescence mapping images of crystals in different z positions. The color scale corresponds to emission intensities increasing from blue to red.

The emission intensities (indicated by the color scale) decreased as the focal point was shifted towards the crystals, being characterized by green and blue colors. It is worth pointing out that such measurements were performed in a 3D mode, and the resulting curves represent the average data from both phases.

The photoluminescence was also mapped with excitation centered at 1064 nm. Such wavelength corresponds to the tail of the absorption band of Yb^{3+} ions in the infrared region, as can be seen in Fig. SM1. The band centered at 980 nm is quite large and appears extended to approximately 800 nm at room temperature. This enables the direct energy transfer from Yb^{3+} to Tm^{3+} ions, resulting in the emission around 800 nm shown in Fig. 9a. This band arises mainly from $^3H_4 \rightarrow {}^3H_6$ transition of Tm^{3+} ions [27]. We could not rule out any contribution from level $^4I_{9/2} \rightarrow {}^4I_{15/2}$ transitions of Er^{3+} ions, however, the direct emission of Tm is expected to be much more intense than those from Er^{3+} [26], [27]. We also observed an opposite behavior from Fig. 8a, and the most intense signals were observed for glassy phase rather than for the crystals, corroborating with the fact that the rare earth ions were also dispersed within the glassy phase.

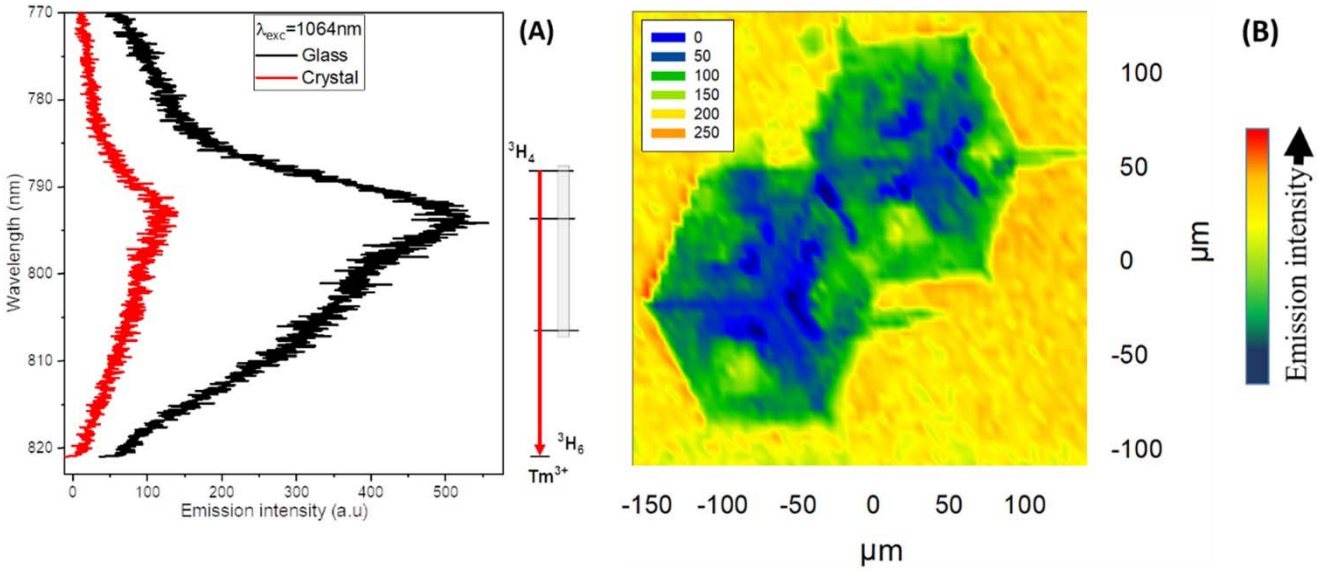

Fig. 9. a) Upconversion spectra from glass and crystals under excitation at 1064 nm. The insert shows the energy levels of Tm^{3+} ions involved in the emission process. b) Luminescence map obtained at 1064 nm. The color scale corresponds to emission intensities increasing from blue to red.

As already discussed, this work aimed to obtain transparent glass-ceramics containing rare earth-doped active crystals. The relative content of rare earths was set at 2 mol% of Yb_2O_3, 0.5 of Er_2O_3 and 0.5 of Tm_2O_3 due to the well-known fact that Yb^{3+} ions are good IR sensitizers for the upconversion photoluminescence of Er^{3+} and Tm^{3+} ions [28], [29]. To study the upconversion effect, the sample PGBG6 was excited using a solid-state laser at 980 nm and the upconversion emission curves are shown in Fig. 10. When upconversion takes place emissions can be expected from the excited state of Er^{3+} and Tm^{3+}. From upper levels of Er^{3+}, emission involving a two-photon absorption process result in signals in the green (525 and 550 nm) and red (660 nm) regions, corresponding to $^2H_{11/2}\rightarrow{}^4I_{15/2}$, $^4S_{3/2}\rightarrow{}^4I_{15/2}$ and $^4F_{9/2}\rightarrow{}^4I_{15/2}$ transitions, respectively. We would also expect two upconversion emissions (at 480 and 800 nm) arising from Tm^{3+} ions, as already observed in other glass systems [26], [27], [30], however, in our case, the blue emission corresponding to $^1G_4\rightarrow{}^3H_6$ transition is very weak, but it could still be observed at ~480 nm [27]. A three-photon process could also originate an upconversion emission from Er^{3+} ions at 410 nm (transition $^2H_{9/2}\rightarrow{}^4I_{15/2}$), but this emission was not detected in our experiments. The week blue emission of Tm^{3+} can be explained by two effects: The first one is related to competition for photons with the Er^{3+} ions. The emission at 480 nm corresponding to Tm^{3+} is a three-photon dependent process, whereas the upconversion concerning the Er^{3+} ions is two-photon dependent process. The second effect is that the absorption tail of the glass matrix falls in the same region where emissions occur, as revealed in Fig. SM1. These two combined effects could explain the low emission intensity of thulium in the blue region. On the other hand, the near infrared emission of Tm^{3+} is very intense and observed at ~800 nm ($^1G_4\rightarrow{}^3H_5$) being concomitant with the emission of Er^{3+}, as explained above. However, the higher intensity of this band can indicate a direct energy transfer from Yb^{3+} to Tm^{3+} ions, thus favoring the photoluminescence emission. Fig. 10b shows the well-known Er^{3+} emission (downshifting) centered at 1550 nm in the near infrared after excitation at 980 nm, corresponding to the $^4I_{13/2}\rightarrow{}^4I_{15/2}$ transition. A broad emission band was observed, corresponding to erbium ions in the amorphous phase, along with sharper emissions around 1535 and 1554 nm ascribed to the stark levels of erbium incorporated in the crystalline phases. These results demonstrate that both upconversion and downshifting processes happen simultaneously and compete for photons, but the green upconversion emission is still high, as can be seen in Fig. 11. The microscope image shows the green emission arising mainly from crystalline phase when the sample is excited at 980 nm with a solid-state laser. This observation corroborates with the statements discussed in this paper that the rare earths were embedded both in the crystalline and glassy phases.

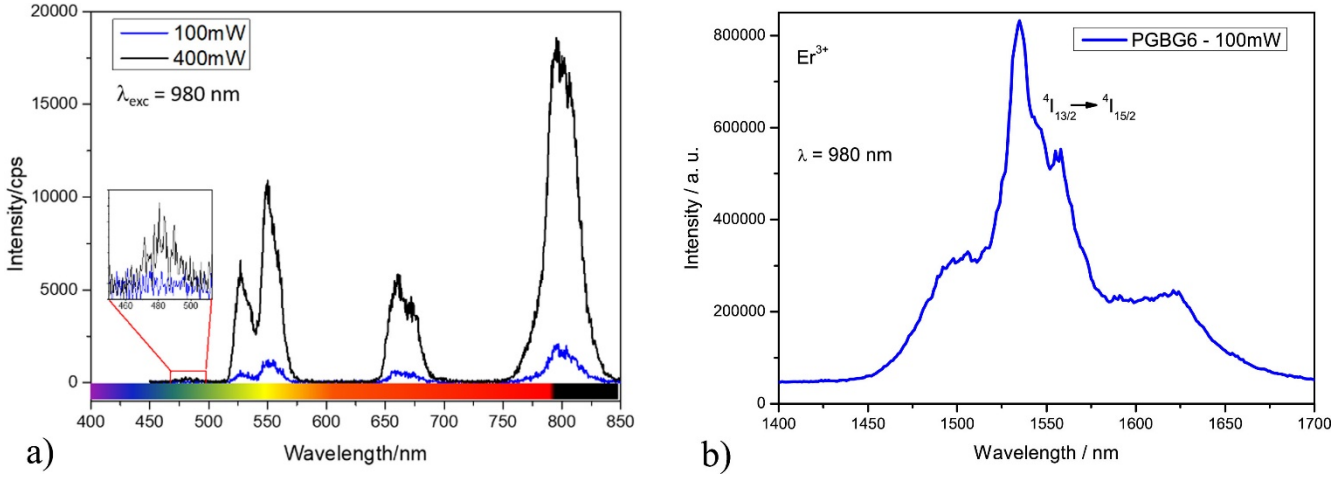

Fig. 10. a) Upconversion spectra of PGBG6 containing Er^{3+}/Tm^{3+}-doped gallate crystals under excitation at 980 nm with two different potencies. The insert shows the low intensity upconversion of Tm^{3+} at 480 nm. b) Near infrared downshifting emission of Er^{3+} ions.

The emissions arising from Er^{3+} and Tm^{3+} ions are of practical interest. While erbium-doped systems have been largely used as probes in nanothermometers (using the upconversion effect) [31], [32] and telecom systems (downshifting) [33], Tm^{3+} have been studied for white light generation [30] and bioimaging in the near infrared (750–1000 nm) of biological tissues due to deeper light penetration and higher image contrast [34], [35]. Concerning the energy level diagram, the mechanisms for energy transfer from Yb^{3+} towards both Er^{3+} and Tm^{3+} ions are well-known [36], [37], [38]. Fig. 12 summarizes all emissions that were discussed herein throughout this manuscript.

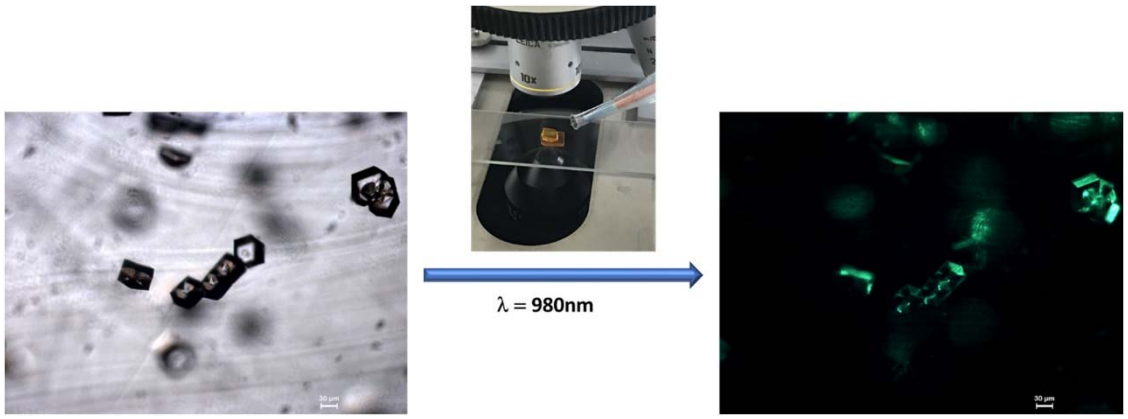

Fig. 11. Microscope images of glass-ceramic sample (PGBG6) before (left image) and during (right image) exposure to 980 nm solid state laser (shown in the center). Green light corresponds to upconversion emissions of Er^{3+} ions mainly incorporated in the crystalline phase.

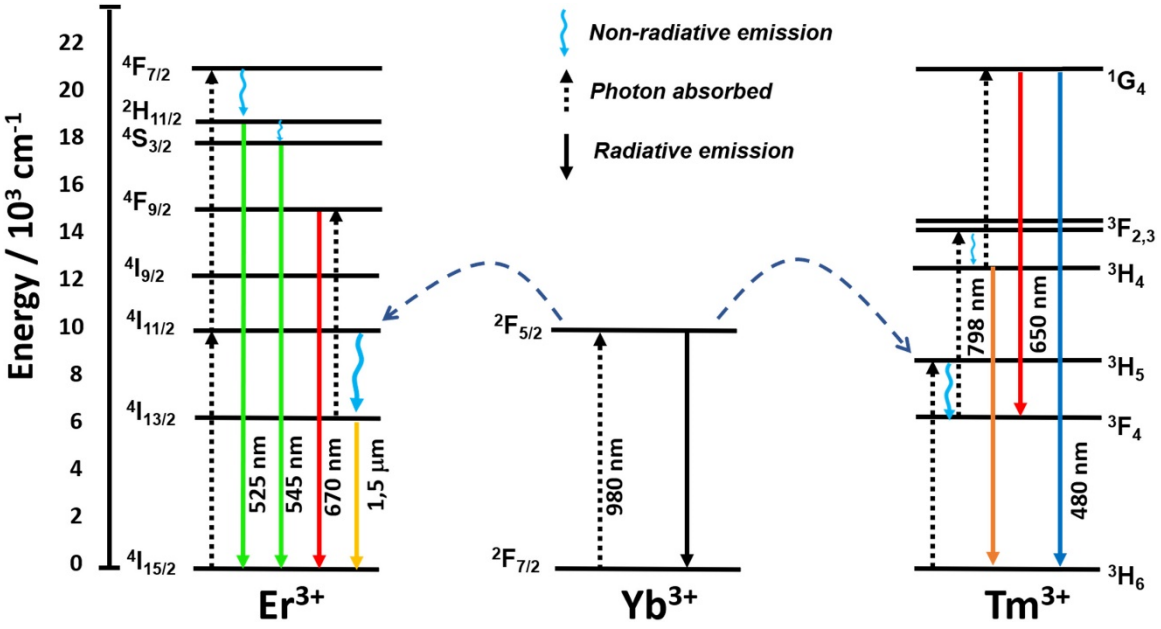

Fig. 12. Energy level scheme of Yb^{3+}/Er^{3+} and Yb^{3+}/Tm^{3+} under excitation at 980 nm demonstrating both upconversion and downshifting processes.

4. Conclusions

This study demonstrates the possibility of obtaining Er^{3+}/Tm^{3+}-doped cubic $Yb_3Ga_5O_{12}$ single-crystals dispersed in a germano-gallate glass system. Crystals with sizes ranging from 10 to 150 µm were obtained. The REE were present as substitutes of Yb in the crystal lattice. Both glassy and crystal phases exhibited emissions from the RE ions. Upconversion in the visible and near infrared ranges was observed when the glass-ceramic was excited at 980 nm. These materials displayed high sensitivity, thus being promising candidates as optical thermometers and devices for near infrared imaging.

CRediT authorship contribution statement : Antonio E. Souza: Performed the experiments and wrote the draft. **Selma G. Antônio**: Performed XRD and simulation studies. **Sidney J.L. Ribeiro**: Supervised the luminescent measurements and help in the discussion. **Douglas F. Franco**: Performed Raman measurements and discussion of the data. **Gustavo Galeani**: Performed luminescence measurements and help in the discussion. **Marc Dussauze**: Performed micro-luminescence measurements and treated the data and corrected the paper. **Thierry Cardinal**: Participated in the discussion of the manuscript and corrected the text. **Marcelo Nalin**: Writing, Editing and Reviewing.

Declaration of Competing Interest : The authors declare that they have no known competing financial interests or personal relationships that could have appeared to influence the work reported in this paper.

Acknowledgments : The authors acknowledge São Paulo Research Foundation - FAPESP (Brazil) grant numbers 2013/07793-6 and 2019/01223-0 and Conselho Nacional de Desenvolvimento Cientfico e Tecnologico - CNPq (Brazil) (502391/2014-6) for the financial support.

Appendix A. Supplementary material

References

1. K. Yoshimoto, A. Masuno, M. Ueda, H. Inoue, H. Yamamoto, T. Kawashima. **Low phonon energies and wideband optical windows of La_2O_3-Ga_2O_3 glasses prepared using an aerodynamic levitation technique.** Sci. Rep., 7 (2017), p. 45600, 10.1038/srep45600

2. D. Manzani, J.F.S. Petruci, K. Nigoghossian, A.A. Cardoso, S.J.L. Ribeiro. **A portable luminescent thermometer based on green up-conversion emission of Er^{3+}/Yb^{3+} co-doped tellurite glass.** Sci. Rep., 7 (2017), p. 41596, 10.1038/srep41596

3. F. Li, W. Zhang, B. Ma, Z. Lu, J. Qi. **Transparent Ce:Y3Al5O12 ceramic phosphors for white light-emitting diodes.** Appl. Phys. Lett., 101 (2012), Article 061902, 10.1063/1.4742896

4. K. Hirao, T. Mitsuyo, J. Si, J. Qiu. **Active glass for photonic devices: photoinduced structures and their application.** Springer Series in Photonics, 7, Springer (2001), pp. 90-91, 10.1007/978-3-662-04603-6

5. V. Venkatramu, M. Giarola, G. Mariotto, S. Enzo, S. Polizzi, C.K. Jayasankar, F. Piccinelli, M. Bettinelli, A. Speghini. **Nanocrystalline lanthanide-doped $Lu_3Ga_5O_{12}$ garnets: interesting materials for light-emitting devices.** Nanotechnology, 21 (2010), Article 175703, 10.1088/0957-4484/21/17/175703

6. H.-J. Reyher, B. Faust, B. Sugg, R. Rupp, L. Ackermann. **Optically detected magnetic resonance via the magnetic circular dichroism of absorption of cerium impurities in bulk paramagnetic terbium gallium garnet.** J. Phys. Condens. Matter, 9 (1997), pp. 9065-9082, 10.1088/0953-8984/9/42/020

7. V. Venkatramu, S.F. León-Luis, U.R. Rodríguez-Mendoza, V. Monteseguro, F.J. Manjón, A.D. Lozano-Gorrín, R. Valiente, D. Navarro-Urrios, C.K. Jayasankar, A. Muñoz, V. Lavín. **Synthesis, structure and luminescence of Er^{3+} doped $Y_3Ga_5O_{12}$ nano-garnets.** J. Mater. Chem., 22 (2012), pp. 13788-13799, 10.1039/c2jm31386c

8. J.A.M. Paddison, H. Jacobsen, O.A. Petrenko, M.T. Fernández-Díaz, P.P. Deen, A.L. Goodwin. **Hidden order in spin-liquid $Gd_3Ga_5O_{12}$.** Science, 350 (2015), pp. 179-181, 10.1126/science.aaa5326

9. R. Krsmanović, V.A. Morozov, O.I. Lebedev, S. Polizzi, A. Speghini, M. Bettinelli, G. Van Tendeloo. **Structural and luminescence investigation on gadolinium gallium garnet nanocrystalline powders prepared by solution combustion synthesis.** Nanotechnology, 18 (2007), Article 325604, 10.1088/0957-4484/18/32/325604

10. Y. Zorenko, V. Gorbenko, T. Voznyak, V. Savchyn, S. Nizhankovskiy, A. Dan'ko, V. Puzikov, V. Laguta, J.A. Mares, M. Nikl, K. Nejezchleb, M. Batentschuk, A. Winnacker. **Luminescent and scintillation properties of $Lu_3Al_5O_{12}$:Sc single crystal and single crystalline films.** Opt. Mater., 34 (2012), pp. 2080-2085, 10.1016/j.optmat.2012.04.018

11. A.V. Kir'yanov, V. Aboites, A.M. Belovolov, M.I. Timoshechkin, M.I. Belovolov, M.J. Damzen, A. Minassian. **Powerful visible (530–770 nm) luminescence in Yb,Ho:GGG with IR diode pumping.** Opt. Express, 10 (2002), pp. 832-839, 10.1364/OE.10.000832

12. C. Stewen, M. Larionov, A. Giesen, K. Contag. **Yb:YAG thin disk laser with 1 kW output power.** Adv. Solid State Lasers, 34 (2000), pp. 35-41, 10.1364/ASSL.2000.MA5

13. E.C. Honea, R.J. Beach, S.C. Mitchell, J.A. Skidmore, M.A. Emanuel, S.B. Sutton, S.A. Payne. **High-power dual-rod Yb:YAG laser.** Opt. Lett. (2000), pp. 805-807, 10.1364/OL.25.000805

14. Q.Y. Zhang, T. Li, D.M. Shi, G.F. Yang, Z.M. Yang, Z.H. Jiang. **Effects of PbF_2 doping on structure and spectroscopic properties of Ga_2O_3–GeO_2–Bi_2O_3–PbO glasses doped with rare earths.** J. Appl. Phys., 99 (2006), pp. 033510-033514, 10.1063/1.2169874

15. G. Yang, T. Li. **Broadband 1.53 μm emission in Er^{3+}-doped Ga-Bi-Pb-Ge heavy metal oxide glasses.** J. Rare Earths, 26 (2008), pp. 924-927, 10.1016/S1002-0721(09)60035-1

16. C. Liu, Z. Xia, M.S. Molokeev, Q. Liu. **Synthesis, crystal structure, and enhanced luminescence of garnet-type $Ca_3Ga_2Ge_3O_{12}$:Cr^{3+} by codoping Bi^{3+}.** J. Am. Ceram. Soc., 98 (2015), pp. 1870-1876, 10.1111/jace.13553

17. K. Fukumi, T. Kokubo, K. Kamiya, S. Sakka. **Structures of alkali niobium gallate glasses.** J. Non-Cryst. Solids, 84 (1986), pp. 100-104, 10.1016/0022-3093(86)90766-0

18. D.M. McKeown, C.I. Merzbacher. **Raman spectroscopic studies of BaO-Ga_2O_3-GeO_2 glasses.** J. Non-Cryst. Solids, 183 (1995), pp. 61-72, 10.1016/0022-3093(94)00648-2

19. M. Montesso, D. Manzani, J.P. Donoso, C.J. Magon, M. Nalin. **Synthesis and structural characterization of a new $SbPO_4$-GeO_2 glass system.** J. Non-Cryst. Solids, 500 (2018), pp. 133-140, 10.1016/j.jnoncrysol.2018.07.005

20. M. Subhadra, P. Kistaiah. **Infrared and Raman spectroscopic studies of alkali bismuth borate glasses: evidence of mixed alkali effect.** Vib. Spectrosc., 62 (2012), pp. 23-27, 10.1016/j.vibspec.2012.07.001

21. M.C. Saine, E. Husson, H. Brusset. **Etude vibrationnelle d'aluminates et de gallates de terres rares-III. Aluminates et gallates de structure grenat.** Spectrochim. Acta, 38A (1982), pp. 25-29, 10.1016/0584-8539(82)80173-6

22. F. Miyaji, S. Sakka. **Structure of PbO-Bi_2O_3-Ga_2O_3 glasses.** J. Non-Cryst. Solids, 134 (1991), pp. 77-85, 10.1016/0022-3093(91)90013-V

23. S.Q. Man, E.Y.B. Pun, P.S. Chung. **Praseodymium-doped alkali bismuth gallate glasses.** J. Opt. Soc. Am. B, 17 (2000), pp. 23-27, 10.1364/JOSAB.17.000023

24. T. Guèrineau, C. Strutynski, T. Skoak, S. Morency, A. Hanafi, F. Calvazala, Y. Ledemi, S. Danto, T. Cardinal, Y. Messaddeq, E. Fargin. **Extended germano-gallate fiber drawing domain: from germanates to gallates optical fibers.** Opt. Mater. Express, 9 (2019), pp. 2437-2445, 10.1364/OME.9.002437

25. S. Li, Y. He, F. Zeng, X. Wang, C. Sun, Z. Su. **Tunable magnetic and fluorescent properties of Tb3Ga5O12 nanoparticles doped with Er3+, Yb3+ and Sc3+.** J. Alloy. Compd., 794 (2019), pp. 227-235, 10.1016/j.jallcom.2019.04.171

26. D. Kasprowicz, M.G. Brik, A. Majchrowski, E. Michalski, P. Gluchowski. **Up-conversion emission in $KGd(WO_4)_2$ single crystals triply-doped with Er^{3+}/Yb^{3+}, $Tb^{3+}/Yb^{3+}/Tm^{3+}$ and $Pr^{3+}/Yb^{3+}/Tm^{3+}$ ions.** Opt. Mater., 33 (2011), pp. 1595-1601, 10.1016/j.optmat.2011.04.038

27. A.M. Babu, B.C. Jamalaiah, T. Chengaiah, G.V.L. Reddy, L.R. Moorthy. **Upconversion luminescence in Tm^{3+}/Yb^{3+} co-doped lead tungstate tellurite glasses.** Physica B, 406 (2011), pp. 3074-3078, 10.1016/j.physb.2011.05.010

28. C. Strohhöfer, A. Polman. **Absorption and emission spectroscopy in Er^{3+}–Yb^{3+} doped aluminum oxide waveguides.** Opt. Mater., 21 (2003), pp. 705-712, 10.1016/S0925-3467(02)00056-3

29. F. Auzel. **Upconversion and anti-stokes processes with f and d ions in solids.** Chem. Rev., 104 (2004), pp. 139-174, 10.1021/cr020357g

30. Y. Ledemi, D. Manzani, S.J.L. Ribeiro, Y. Messaddeq. **Multicolor up conversion emission and color tunability in $Yb^{3+}/Tm^{3+}/Ho^{3+}$ triply doped heavy metal oxide glasses.** Opt. Mater., 33 (2011), pp. 1916-1920, 10.1016/j.optmat.2011.03.029

31. C.D.S. Brites, P.P. Lima, N.J.O. Silva, A. Millán, V.S. Amaral, F. Palacio, L.D. Carlos. **Thermometry at the nanoscale.** Nanoscale, 4 (2012), pp. 4799-4829, 10.1039/C2NR30663H

32. S. Cui, G. Chen. **Enhanced up-conversion luminescence and optical thermometry characteristics of Er3+/Yb3+ co-doped Sr10(PO4)6O transparent glass-ceramics.** J. Am. Ceram. Soc., 103 (2020), pp. 6932-6940, 10.1111/jace.17418

33. M. Nalin, S.J.L. Ribeiro, D. Manzani, R.R. Gonçalvez, G. Poirier, F.C. Cassanges, C.J.S. Matos, C.R. Mendonça, L. Boni, L. Misoguti, O. Malta, Y. Ledemi, S. Messaddeq, Y. Messaddeq. **Materiais Vítreos e Luz: Parte 2.** Quím. Nova, 39 (2016), pp. 340-351, 10.5935/0100-4042.20160017

34. M. Nyk, R. Kumar, T.Y. Ohulchanskyy, E.J. Bergey, P.N. Prasad. **High contrast in vitro and in vivo photoluminescence bioimaging using near infrared to near infrared up-conversion in Tm^{3+} and Yb^{3+} doped fluoride nanophosphors.** Nano Lett., 8 (2012), pp. 3834-3838, 10.1021/nl802223f

35. E.J. Nassar, S.B. Moscardini, S. Lechevallier, M. Verelst, B. Borak, L.A. Rocha. **Niobium oxide doped with Tm^{3+} and Gd^{3+} ions for multimodal imaging in biology.** J. Sol-Gel Sci. Technol., 93 (2020), pp. 546-553, 10.1007/s10971-019-05213-x

36. J. Méndez-Ramos, V.D. Rodriguez, V.K. Tikhomirov, J. del-Castillo, A.C. Yanes. **Yb^{3+}-Er^{3+}-Tm^{3+} co-doped nano-glass-ceramics tuneable up-conversion phosphor.** Eur. Phys. J. Appl. Phys., 43 (2008), pp. 149-153, 10.1051/epjap:2008101

37. H. Wang, X. Hong, R. Han, J. Shi, Z. Liu, S. Liu, Y. Wang, Y. Gan. **Triple-doped $KMnF_3$:$Yb^{3+}/Er^{3+}/Tm^{3+}$ nanocubes: four-color upconversion emissions with strong red and near-infrared bands.** Sci. Rep., 5 (2015), p. 17088, 10.1038/srep17088

38. X. Mateos, R. Solé, Jna Gavaldà, M. Aguiló, F. Díaz, J. Massons. **Ultraviolet and visible emissions of Er^{3+} in $KY(WO_4)_2$ single crystals co-doped with Yb^{3+} ions.** J. Lumin., 115 (2005), pp. 131-137, 10.1016/j.jlumin.2005.01.015